D2.7

QE and SIESTA workflows for advanced materials parameters (Task 2.2.3-5): Part 2

Arsalan Akhtar, Alberto García, Roberta Farris, Pablo Ordejón, Miguel Pruneda, Linda-Sheila Medondjio, Flaviano J. dos Santos, Luca Bursi, Arrigo Calzolari, and Nicola Marzari

Document information

Project acronym:	INTERSECT
Project full title:	Interoperable Material-to-Device simulation box for disruptive electronics
Research Action Project type:	Accelerating the uptake of materials modeling software (IA)
EC Grant agreement no.:	814487
Project starting / end date:	1st January 2019 (M1) / 30th April 2022 (M40)
Website:	www.intersect-project.eu
Final version:	27/04/2022
Deliverable No.:	D2.7
Responsible participant:	EPFL (participant number 2)
Contributing Consortium members:	ICN2, CNR
Due date of deliverable:	30/04/2022
Actual submission date:	29/04/2022
Dissemination level:	PU - Public
Authors:	Arsalan Akhtar, Alberto García, Roberta Farris, Pablo Ordejón, Miguel Pruneda, Linda-S. Medondjio, Flaviano J. dos Santos, Luca Bursi, Arrigo Calzolari, Nicola Marzari
To be cited as:	A. Akhtar, A. García, R. Farris, P. Ordejón, M. Pruneda, L.-S. Medondjio, F. J. dos Santos, L. Bursi, A. Calzolari, and N. Marzari (2022): "QE and SIESTA workflows for advanced materials parameters (Task 2.2.3-5): Part 2". Deliverable D2.7 of the H2020 project INTERSECT (final version as of 27/04/2022). EC grant agreement no: 814487, EPFL, Lausanne, Switzerland

Disclaimer:

European Commission has no liability in respect of this document, which is merely representing the authors' view.

Versioning and Contribution History

Version	Date	Modified by	Modification reason
v.01	19/04/2022	Alberto Garcia	First version
v.02	21/04/2022	Flaviano Dos Santos and Luca Bursi	First revision
v.03	21/04/2022	Arrigo Calzolari	Second revision
v.04	25/04/2022	Flaviano dos Santos	Third revision
v.05	27/04/2022	Pablo Ordejon	Final version

Content

[1] Acronyms are marked in purple in the text and defined at the end of the document.

1 Executive Summary

The Interoperable Material to Device (IM2D) simulation box for the on-demand calculation of materials properties is at the core of the INTERSECT [1] project. The syntactic infrastructure for such capability is provided by AiiDA [2] through the availability of optimized workflows.

In this document, that updates and complements the content of deliverable D2.2[2] (M13) and D2.3[3] (M25), we present the AiiDA workflows for materials properties implemented as part of INTERSECT with particular focus on the features designated to provide more advanced materials properties. AiiDA infrastructure manages the data pipeline and process workflows; Quantum ESPRESSO (QE) [3] and SIESTA [4] are the Density Functional Theory (DFT) engines used for the actual calculation of the materials properties. The list of implemented materials on demand already reported in Deliverables D2.2 and D2.3 included: total energy, energy band structure, energy band gap, effective mass, dielectric function, (charged) defect formation energy [5], and NEB [6]. Here, we report on further advances in the calculation of those properties and on the implementation of other properties, namely thermal transport and coupled electron-phonon transport in solids. Finally, we will discuss the status and the main issues related to the remaining proposed properties on demand, which are still in progress.

Within the INTERSECT project, most of implemented materials properties on demand are made available to the GINESTRA® code [7], through aiida-ginestra plugin (see also D2.1[4] and D2.4[5]) to upscale the device-oriented GINESTRA® code to advanced materials properties (materials-to-device and device-to-materials interoperable pathways).

2 Introduction

The AiiDA infrastructure is designed to automate the computation of materials properties from first principles calculations through the use of highly-optimized automated workflows. In the context of the INTERSECT project, the AiiDA workflows are exploited towards establishing a control centre for computation as well as for exchange of information – for both, input and

[2] https://intersect-project.eu/wp-content/uploads/2022/04/D2.2.pdf
[3] https://intersect-project.eu/wp-content/uploads/2022/04/D2.3.pdf
[4] https://intersect-project.eu/wp-content/uploads/2022/04/D2.1.pdf
[5] https://intersect-project.eu/wp-content/uploads/2022/04/D2.4.pdf

output quantities – between the quantum mechanical simulation tools (QE and SIESTA) and the GINESTRA® software for atomistic and continuum modeling of electronic devices.

Algorithms for the AiiDA workflows have been designed to fit the needs of the INTERSECT project, as for example in the choice of the physical parameters required for the simulation of the properties of the electronic device (see D1.1[6]). The present deliverable complements the description in D2.2 and D2.3 of the implementation of specific workflows for advanced on-demand properties.

2.1 About this document

This document represents the deliverable D2.7 of the INTERSECT project and it is prepared under the Task 2.2. "Simulation hub: Automated workflows for materials' data on demand of Work Package 2 – Interconnection and Interoperability Implementations". The content of this document is intended to complement D2.2 and D2.3 where the general structure of AiiDA workflows and specific workflows for advanced on-demand properties were described.

It is worth noticing that, as for the case of the defect formation energy and the diffusion barrier, the properties discussed in this deliverable (e.g., first principles evaluation of the thermal transport in solids or the electron-phonon coupling) are very high-level tasks, whose theoretical models and their code implementation are still top challenges in current scientific research. On the one hand, this requires some advanced skills in the use of the implemented workflows. On the other hand, it represents a net step forward in characterization of the "material at the device level" and a unique tool that distinguishes IM2D from the existing device-oriented codes.

3 QE and SIESTA workflows for advanced properties

3.1 Update to the workflows for automated determination of diffusion barriers of defects and impurities in materials

Following the anticipated roadmap outlined in D2.3, the workflows for the automated determination of diffusion barriers (Task 2.2.4) have now been packaged in a new plugin, aiida-

[6] https://intersect-project.eu/wp-content/uploads/2022/04/D1.1.pdf

siesta-barrier[7]. The workflows in this package implement functionality for specific processes (interstitial diffusion, exchange, vacancy exchange) and call the appropriate lower-level workflows in the aiida-siesta package.

3.2 Update to the workflows for the calculation of the formation energy of (charged) defects

The QE-related workflow family has been improved and refined, going a few steps further in the process of making AiiDA-Defect more flexible and more user friendly. The package has been updated to improve robustness and some internal default values have been set. Extra functionalities have been added to the workchain that automatically determines the stability ranges of elemental chemical potentials in a selected defect calculation (Sec. 4.8 in D2.3). Now, two separate dictionaries have to be provided in input, one containing the reference values of the chemical potentials for the elements composing the material (obtained from total energy DFT calculations), and one containing the formation energies of the stable parent compounds, obtainable from databases available online through a simple python script.

We extended the capability of the 'GaussianCountercharge' workchain. The original version (see Sec. 4.8 in D2.3) implemented the KP-FNV scheme employing the standard “Gaussian model charge” approach. Now, a more advanced technique has been developed: the charge density associated with the defect is obtained as the difference between the charge densities of the defective and the pristine systems. Furthermore, we extended the 'GaussianCountercharge' workchain to work with dielectric tensors that are not necessarily diagonal as in the initial implementation.

Finally, the SIESTA version of these workflows now implements similar improvements over the standard “Gaussian model charge” approach. These are necessary when the charge density associated with the defect is not sufficiently compact.

3.3 Update on effective masse workflow

We have further developed the effective mass workflow. Previously, this AiiDA workflow computed the effective mass only along the high-symmetry lines of the band structure. With the new update, it is possible to compute the entire 3x3 effective mass tensors M^*_{ij} in any k_0 point of the 3D Brillouin zone:

[7] https://github.com/siesta-project/aiida-siesta-barrier

$$M^*_{n,ij}(\boldsymbol{k_0}) = \frac{\hbar^2}{m_0}\left(\frac{\partial^2 E_n(\boldsymbol{k})}{\partial k_i \partial k_j}\right)^{-1}_{\boldsymbol{k_0}}$$

This is done by considering the full mathematical complexity of the overall 3D band structure $E_n(\mathbf{k})$, and not simply along the 2D band structure plots. A numerical automatic fitting of the band energies is done by using 10 free parameters (9 for the effective mass tensor, 3 for the k-point displacement, and 1 for the energy displacement). The band energies are computed in a regular grid around the k-point of interest. This extension allows us to describe the velocity of electrons and holes, most relevant for transport, along any direction in the 3-dimensional space.

3.4 Computation of the thermal conductivity

A number of techniques are available for the calculation of the (lattice) thermal conductivity. They can be roughly divided into two classes: those using molecular-dynamics, and those relying on the computation of the higher-order force constants that determine the phonon-phonon interaction and hence the degradation of the thermal flow. In what follows we describe briefly our implementation of three schemes: the approach-to-equilibrium MD, the Green-Kubo method based on the analysis of the autocorrelation of the thermal flux in equilibrium, and the TDEP method based on the fitting of (renormalized) higher-order force constants to MD-snapshot information.

3.4.1 Approach-to-equilibrium MD

This approach (see [8] and references therein) evaluates the thermal conductivity from the temperature transient regime by using the exact solution of the heat transport equation for an initial steplike temperature profile. The system is initially divided in two halves at different initial temperatures T1 and T2 (Figure 1), and the thermal conductivity is obtained by fitting the temperature difference during the MD simulation to the expected solution of the thermal transport problem:

$$\Delta T(t) = \langle T_1 \rangle - \langle T_2 \rangle = \sum_{n=1}^{\infty} C_n e^{-\alpha_n^2 \bar{\kappa} t}$$

where the $\boldsymbol{\alpha}_n$ are related to the size L_z of the system and the coefficients are given by

$$C_n = 8(T_1 - T_2)\frac{[\cos(\alpha_n L_z/2) - 1]^2}{\alpha_n^2 L_z^2}$$

These quantities can be evaluated from first principles by running ab initio MD simulations with the SIESTA code.

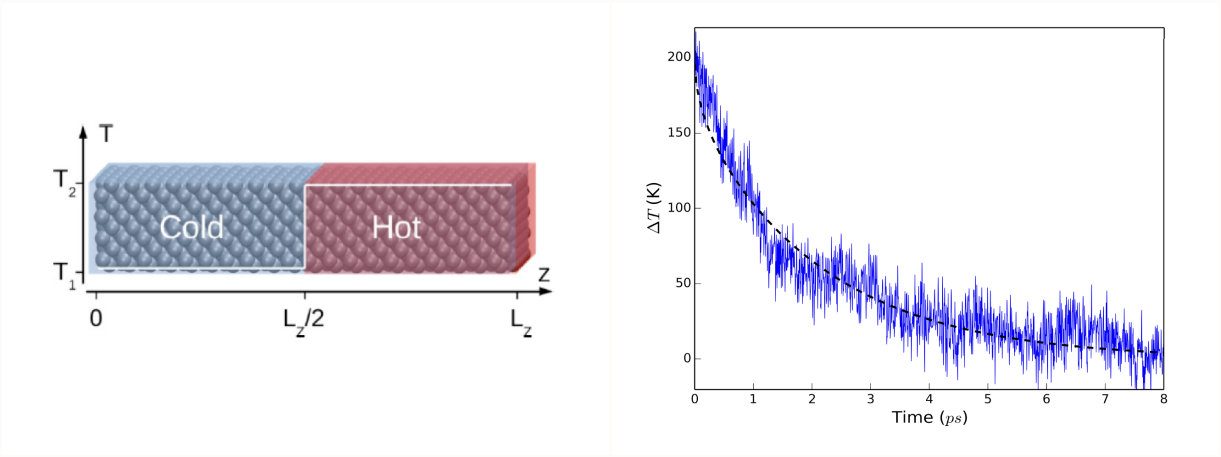

Figure 1. Calculation of thermal conductivity using the Approach to Equilibrium Molecular Dynamics method [8]. Left: Scheme of the preparation of the system imposing a difference in temperature along the simulation cell. Right: Evolution of the difference in temperature with time, which serves to compute the thermal conductivity.

3.4.2 Green-Kubo method

After the seminal work by Marcolongo et al. [9] on the gauge invariance of the conductivity with respect to different choices of the energy density, the Green-Kubo method can be used with first-principles simulations. The Green-Kubo relations connect transport coefficients to the autocorrelation of equilibrium fluctuations in the appropriate fluxes. Hence, the practical scheme involves: running a molecular dynamics simulation, extracting snapshot information, computing the thermal flux for each one, and performing a statistical analysis of the autocorrelation. The MD runs can be conveniently and efficiently done with SIESTA, and the computation of the thermal fluxes can be carried out with either QEHeat [10] (a program based on QE modules) or a special version of SIESTA in which the flux functionality has been implemented. Specifically, the thermal conductivity is given by:

$$\kappa = \frac{1}{Vk_BT^2}\int_0^\infty \langle \hat{J}(t)\hat{J}(0)\rangle dt$$

where the thermal flux J can be computed, within DFT, as the sum of several contributions:

$$\mathbf{J}^E_{DFT} = \mathbf{J}^H + \mathbf{J}^Z + \mathbf{J}^0 + \mathbf{J}^{KS} + \mathbf{J}^{XC}$$

$$\begin{cases} \mathbf{J}^H = \frac{1}{4\pi\Omega e^2}\int \nabla v_H(\mathbf{r})\dot{v}_H(\mathbf{r})d\mathbf{r} \\ \mathbf{J}^Z = \frac{1}{\Omega}\sum_n \left[\mathbf{V}_n\left(\frac{1}{2}M_n V_n^2 + w_n\right) + \sum_{m\neq n}(\mathbf{R}_n - \mathbf{R}_m)\left(\mathbf{V}_m \cdot \frac{\partial w_n}{\partial \mathbf{R}_m}\right)\right] \\ \mathbf{J}^0 = \frac{1}{\Omega}\sum_n\sum_v \left\langle \phi_v \middle| (\mathbf{r}-\mathbf{R}_n)\left(\mathbf{V}_n \cdot \frac{\partial \hat{v}_0}{\partial \mathbf{R}_n}\right)\middle| \phi_v \right\rangle \\ \mathbf{J}^{KS} = \frac{1}{\Omega}\Re_e \sum_v \left\langle \bar{\phi}^c_v \middle| H_{KS} + \varepsilon_v \middle| \dot{\phi}^c_v \right\rangle \\ J^{XC}_\alpha = -\frac{1}{\Omega}\int n(\mathbf{r})\dot{n}(\mathbf{r})\frac{\partial \epsilon^{GGA}(\mathbf{r})}{\partial(\partial_d n)}d\mathbf{r} \quad (GGA) \end{cases}$$

This method is completely general, and it does not make any assumption about the system under consideration. It is particularly suited for the computation of the thermal conductivity in non-crystalline systems (liquids, amorphous solids, etc). On the other hand, it requires the use of appropriately large supercells to describe correctly the thermal fluxes, and, in principle, appropriately long simulation times to compute the involved autocorrelation functions. Note however, that it is possible to frame the statistical analysis in a special way [11], by requiring only moderately long trajectories.

3.4.3 TDEP scheme

TDEP (Temperature-Dependent Effective Potential) is a method (and code implementation) [12] to compute the thermal properties of materials, including the thermal conductivity, which takes into account all the anharmonic effects that renormalize the force constants (including the higher-order ones) as a function of temperature. TDEP uses the information in a series of molecular-dynamics snapshots (coordinates and forces) to fit an effective lattice potential in the form of a Taylor expansion in atomic displacements. The coefficients are then the renormalized force constants. The solution of the Boltzmann transport equation gives the desired properties.

In INTERSECT, we have developed an interface between TDEP and SIESTA, so that all the information needed to compute the thermal properties of the materials through TDEP can be obtained from first-principles calculations done with SIESTA, as shown in Figure 2. This has been implemented in an AiiDA workflow, based on the block diagram shown in Figure 3, which will be released in the near future.

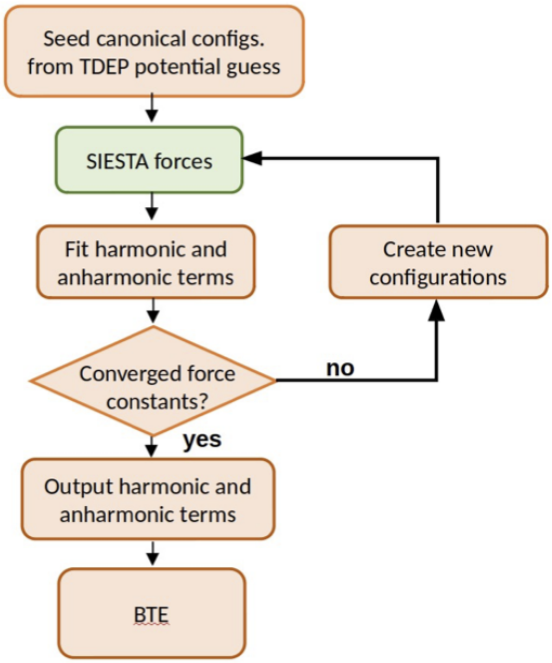

Figure 2. Conceptual scheme of the linking of SIESTA with TDEP, as implemented in the INTERSECT workflow for the calculation of thermal properties of materials. The TDEP driver generates atomic configurations with certain displacements from the equilibrium positions, inquiring SIESTA about the energies and forces for these configurations. TDEP uses these to fit an anharmonic potential. The procedure is iterated until the forces are converged. Finally, the Boltzmann equations are solved to compute the thermal properties (including thermal conductivity).

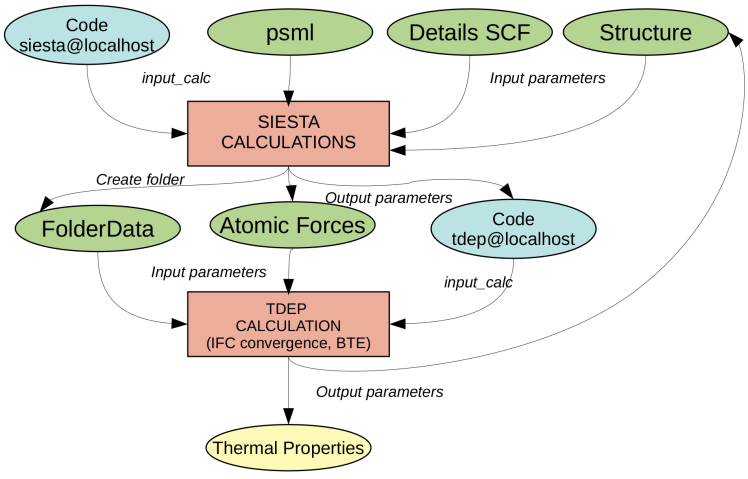

Figure 3. Scheme of the AiiDA workflow orchestrating the calculation of thermal properties of materials through TDEP and SIESTA.

These method and workflow have already been applied to real materials and, in particular, to suspended $MoSe_2$ stacks with different numbers of layers, from the monolayer to the bulk (Figure 4). Our results have been compared to experimental results, thus validating the method [13].

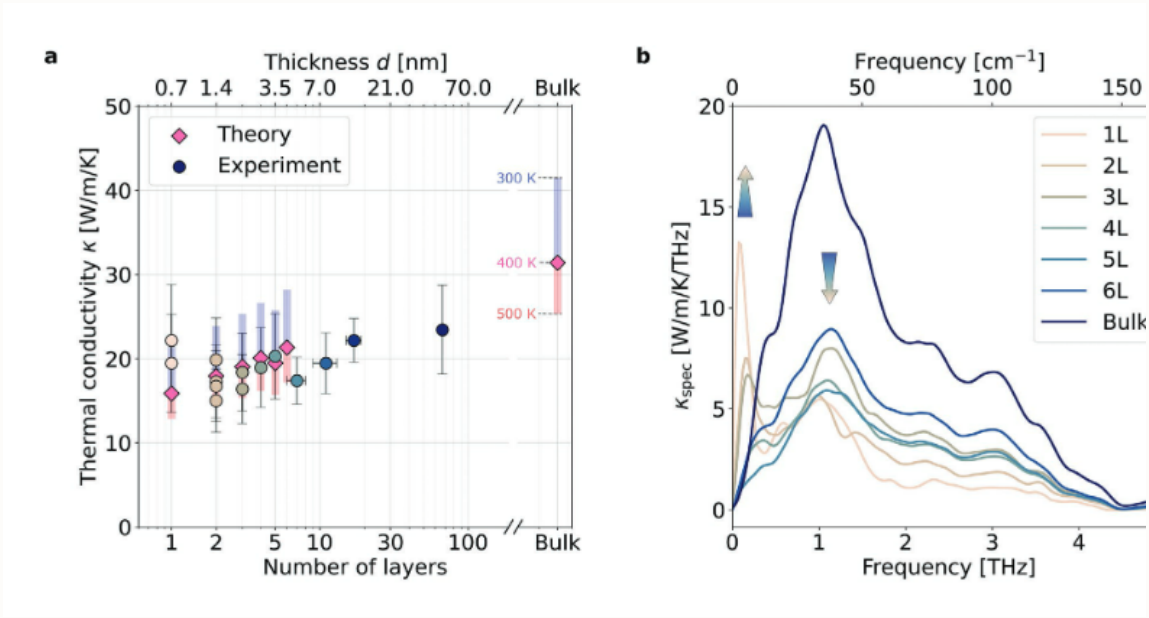

Figure 4. In-plane thermal conductivity of $MoSe_2$ crystals as a function of the number of layers [13]. (a) Comparison of the calculated (red symbols) and experimental (blue symbols). (b) Spectrally decomposed thermal conductivity as a function of phonon frequency, indicating how toward thinner films an increasing contribution from a sub-THz mode compensates the decreasing contribution from modes around 1 THz.

With the results validated with experiments in $MoSe_2$, we have computed the thermal properties of materials relevant to the project, such as GeSe for selectors. We have computed first the phonon Density of States and the thermal conductivity for crystalline GeSe, and then for an amorphous sample developed within the project, in the work of WP3. Figure 5 shows the comparison of the DOS for the crystalline and the amorphous samples. The thermal conductivity of the crystal is shown in Figure 6, as a function of temperature. The conductivity is anisotropic, according to the crystalline symmetry of the materials. The symbol in Figure 6 shows the calculated conductivity of the amorphous sample, at a temperature of 300K. The reduction of the thermal conductivity from the crystal to the amorphous case is quite dramatic, close to a factor of 10.

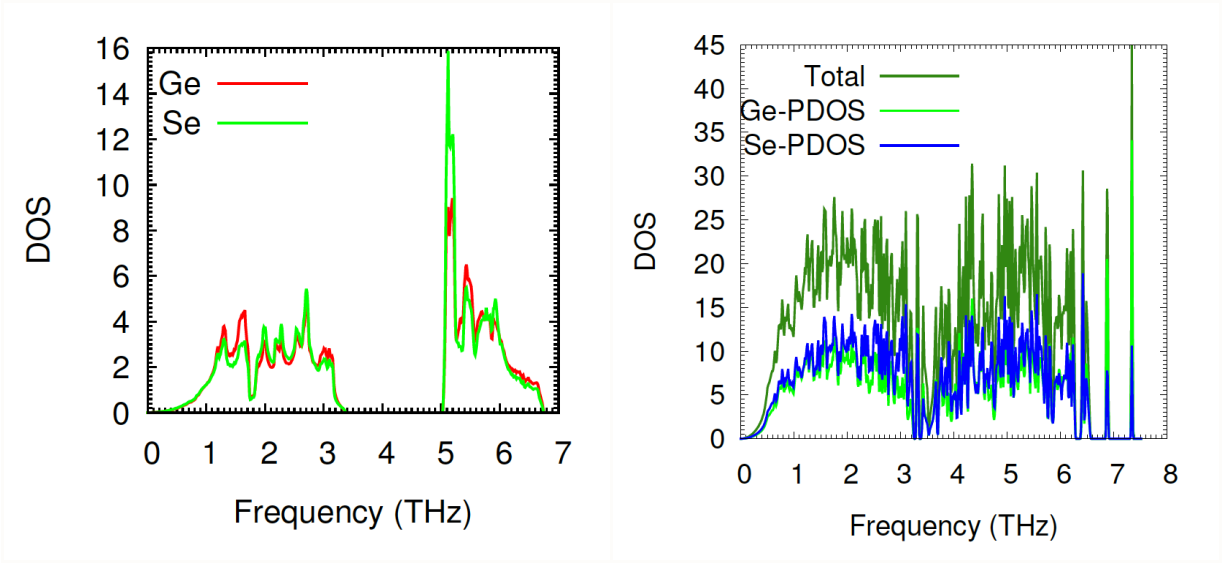

Figure 5. Phonon DOS for crystalline (left) and amorphous (right) GeSe samples, computing with the workflows involving SIESTA and TDEP.

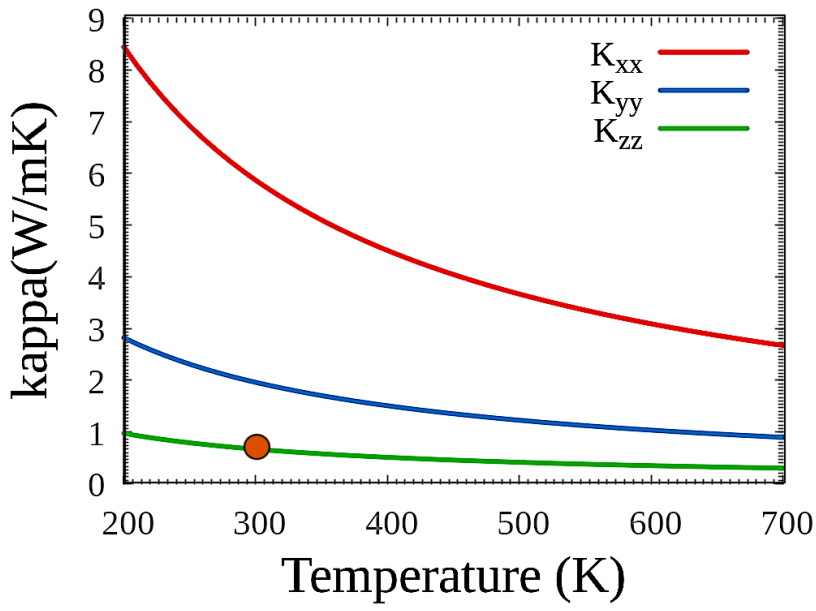

Figure 6. Thermal conductivity of crystalline GeSe, as a function of temperature. The three lines show the conductivity along a different crystalline axis. The symbol shows the conductivity of an amorphous GeSe model.

3.5 Computation of the coupled electrical and thermal conductivity

The computer code ELPHBOLT [14] uses, in addition to the phonon-related force constants, the electron-phonon coupling coefficients, and goes on to solve a *coupled* electron-and-phonon Boltzmann equation. Hence, it can include the effect of the nonequilibrium phonons on the electronic transport (phonon drag) and non-equilibrium electrons on the phononic transport (electron drag) in a fully self-consistent manner and obeying the constraints mandated by thermodynamics. ELPHBOLT can calculate the lattice, charge, and thermoelectric transport coefficients for the temperature gradient and electric fields, and the effect of the mutual electron-phonon drag on these transport properties. ELPHBOLT currently works with QE and EPW to compute and process the force constants and electron-phonon coupling coefficients (Figure 7), but a workflow based on SIESTA (in particular for the electron-phonon couplings) can also be used, employing part of the technology developed in the TDEP scheme presented above. The workflow has already been applied to predict a colossal phonon drag enhancement of the thermopower in lightly doped diamond, as shown in Figure 8 [15].

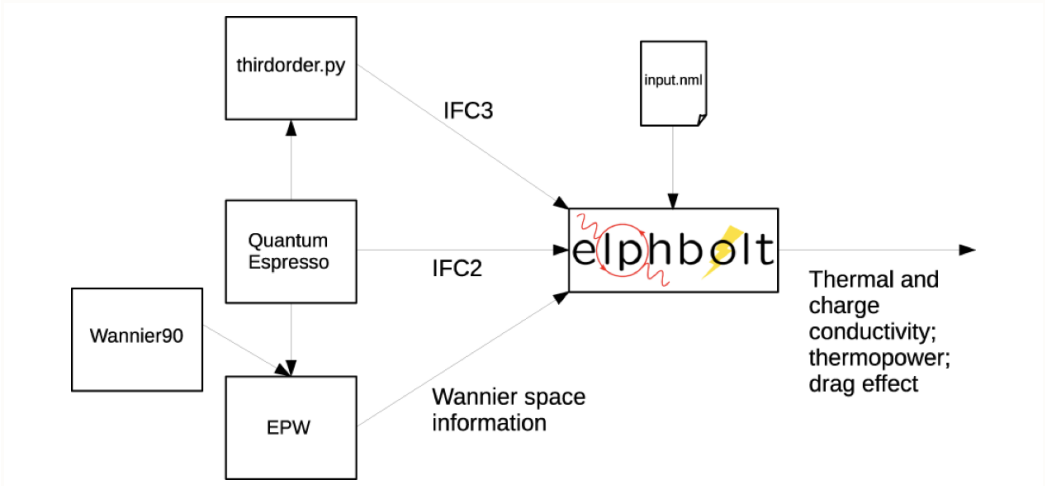

Figure 7. Scheme of the components of the calculation of the coupled thermal and electrical conductivity through ELPHBOLT, and how it links with other (open source) software packages like Quantum ESPRESSO, Wannier90, and EPW [14].

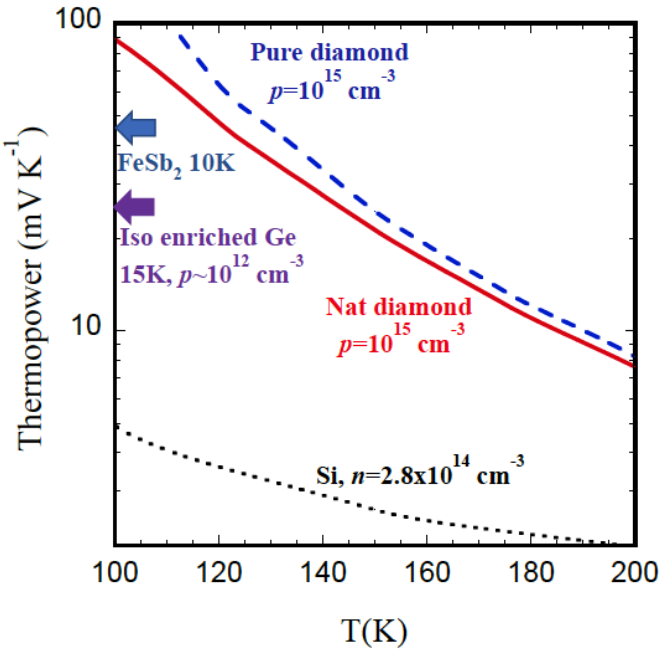

Figure 8. Application of ELPHBOLT to the calculation of the thermopower of p-doped diamond [13]. The red and blue curves show the results for p-doped diamond, both in pure isotope (blue) and natural (red) forms. The results were obtained including the phonon drag, which is shown to enhance the thermopower by a factor of x100, the value when phonon drag is not included being smaller than 1 mVK-1, out of the scale of the graph. We also show for reference the values calculated for silicon, as well as the experimental values for p-doped germanium and FeSb2, the material with the largest experimentally recorded value (but at much lower temperature than our calculations for diamond).

3.6 Work in progress

With respect to the original DoA plan, only two of the eleven properties on demand mentioned in Task 2.2 have not been completely implemented in automated workflows: the work-function and multi-domain wall dynamics. In the following, we report on the present status of these features and the causes of the delay.

3.6.1 Tools for the determination of the structure and dynamics of domain walls

Task 2.2.5 is about the development and implementation of tools for the determination of the structure and dynamics of domain walls in ferroic materials, including the effect of external fields. This subject is particularly relevant for the study of ferroelectric devices, as in pilot case 1 (WP3). However, this is the most explorative (i.e., less advanced) feature we tackled in this project. Indeed, while for the properties discussed above, even though a final solution is not

yet achieved, there was an initial theoretical model to solve the problem (i.e., existing formula to be implemented in the code), in this case the theory background is still missing. Up to now, no reliable model is available in the literature to tackle this problem. Thus, before any possible code implementation we worked on the fundamental theory development, able to describe the dynamics of domain walls at an atomistic level. Unfortunately, we faced a few critical issues and we have not achieved this issue, yet.

With respect to the original idea we had during the proposal preparation, the generation of accurate models for the multi-domain structures resulted to be more complex than expected. As a starting point, we considered the idea to build up a convenient lattice Wannier-function model based on a few modes computed in the cubic phase (Figure 9). Indeed, the phase transition from cubic to tetragonal is ruled by the condensation of a soft-phonon that involves antipolar displacements of the oxygen atoms. However, the tetragonal phase (and all other crystal phases studied) is a local minimum with no unstable soft-phonon modes. Although the distortion from the tetragonal to the orthorhombic polar phase can be decomposed reasonably well into a combination of six symmetry-adapted modes of the cubic phase, the field-induced phase transition from tetragonal to orthorhombic is expected to be first-order, which would require a higher-order expansion of the free energy. The dynamical multiscale modeling of the multi-domain structures will also require to play with several coupled order parameters which requires further analysis.

This task activity has been temporarily interrupted, since the postdoc in charge of this line left earlier than expected. Due to difficulties related to COVID restrictions, recruitment of new personnel has been delayed and we could not find a good candidate to conclude this line.

Even though we did not complete the activity of Task 2.2.5, we do not consider this as a failure for the project. Indeed, as mentioned above, this sub-Task required not only the implementation of a physical feature (as for the other sub-Tasks), but also the development of a brand-new theory branch. The negative pursued attempts brought us in any case useful information on the complexity of the problem we tackled. Alternative approaches are under investigation.

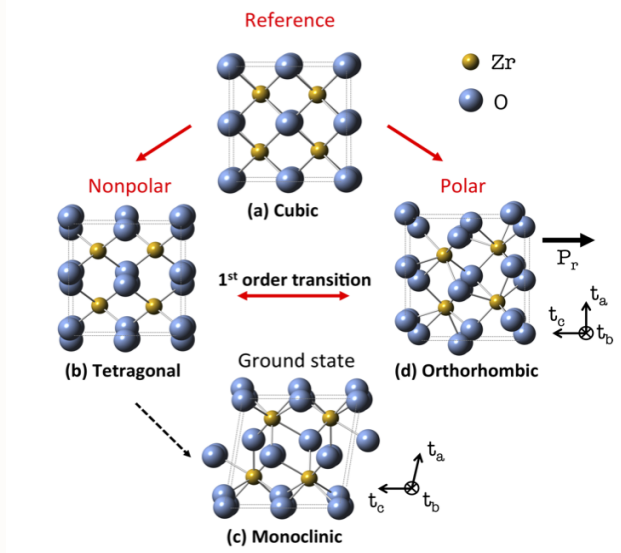

Figure 9. Four crystal structures considered for HfO2. The cubic structure is metastable, with a soft-phonon driving the transition to the tetragonal phase, which is considered as the parent structure for the orthorhombic phase. The low temperature (ground state) phase is the monoclinic one. Picture from Ref. [16].

3.6.2 Work-function

By using the band-offsets between HfO_2 and electrodes as reference testbed (WP3), we started testing the best approach to evaluate the materials work function, through an automatic workflow. We have built the structures, we ran relaxation simulations, and checked what happens with the polar phase in thin films. The methodology however is not completely validated to be finalized into an efficient workflow.

One of the most relevant issues is related to the capability to automatically generate models and extract parameters from surface structures, instead of the crystalline bulk phases needed for all the other considered properties. At present, we have basic building blocks for slab/surface creation, surface relaxation and calculation of the work function and surface energies in an experimental aiida-siesta-surfaces package, but we are still missing a number of refinements needed to create robust and accurate workflows from them, and the estimate of the work-function is too crude to be compared with the experiments. This activity is ongoing.

4 Conclusion

This deliverable reports on the implementation of automatic workflows for the evaluation of advanced materials properties from first principles simulations. This document updates and complements the content of deliverables D2.2 and D2.3. Apart from the continuous refinement process to improve the efficiency of the workflows and/or of the numerical approaches in use to calculate the material parameters, Task 2.2 can be considered mostly completed. With respect to the list of properties mentioned in the DoA (11 entries), nine have been successfully implemented and made available for device simulations in IM2D, through the realization of the corresponding automatic workflows managed by AiiDA. The remaining two advanced properties are in progress.

References

[1] INTERSECT project www.intersect-project.eu.

[2] G. Pizzi, et al., *Comput. Mater. Sci.* **111**, 218 (2016); http://www.aiida.net.

[3] P. Giannozzi, et al., *J. Phys.: Condens. Matter* **21**, 395502 (2009); *J. Phys.: Condens. Matter* **29**, 465901 (2017); http://www.quantum-espresso.org.

[4] J. M. Soler, et al., The SIESTA method for ab initio order-N materials simulation. *J. Phys. Cond.Matt.* **14**, 2745 (2002). SIESTA™ URL https://siesta-project.org/siesta

[5] C. Freysoldt, et al., *Rev. Mod. Phys.* **86**, 253 (2014).

[6] G. Henkelman, et al., *J. Chem. Phys.* **113**, 9901 (2000).

[7] L. Larcher, et al., "A simulation framework for modeling charge transport and degradation in high-k stacks", *J. Comput. Electron.* 12, 658–665 (2013). Ginestra® URL: www.mdlsoft.com.

[8] I. Sergio, et al., "Thermal and Transport Properties of Pristine Single-Layer Hexagonal Boron Nitride: A First Principles Investigation." *Phys. Rev. Mater.* **1** 044006 (2017).

[9] A. Marcolongo, et al., "Microscopic Theory and Quantum Simulation of Atomic Heat Transport." *Nature Physics* **12**, 80–84 (2016).

[10] "QEHeat: An Open-Source Energy Flux Calculator for the Computation of Heat-Transport Coefficients from First Principles", Computer Phys. Commun. **269**, 108090 (2021).

[11] L. Ercole, et al., "Accurate Thermal Conductivities from Optimally Short Molecular Dynamics Simulations." *Sci. Rep.* **7**, 15843 (2017).

[12] O. Hellman and I. A. Abrikosov. "Temperature-Dependent Effective Third-Order Interatomic Force Constants from First Principles." *Phys. Rev. B* **88**, 144301 (2013).

[13] D. S. Reig, et al., "Unraveling Heat Transport and Dissipation in Suspended $MoSe_2$ from Bulk to Monolayer" *Adv. Mater.* **34**, 2108352 (2022).

[14] N. H. Protik, et al., "The Elphbolt Ab Initio Solver for the Coupled Electron-Phonon Boltzmann Transport Equations." *npj Comput. Materi.* **8**, 28 (2022).

[15] C. Li, et al., "Colossal phonon drag enhanced thermopower in lightly doped diamond". *Submitted to PNAS.*

[16] S. E. Reyes-Lillo, et al., "Antiferroelectricity in thin-film ZrO2 from first principles", Phys. Rev. B **90** 140103R (2014).

Acronyms

DFT - Density Functional Theory

DoA - Description of the Action

IM2D – Interoperable Materials-to-Device

QE – Quantum ESPRESSO

TDEP - Temperature-Dependent Effective Potential